AIP | Journal of Applied Physics

CO2 and Er:YAG laser interaction with grass tissues

Jaehun Kim and Hyungson Ki

Citation: J. Appl. Phys. **113**, 044902 (2013); doi: 10.1063/1.4788821
View online: http://dx.doi.org/10.1063/1.4788821
View Table of Contents: http://jap.aip.org/resource/1/JAPIAU/v113/i4
Published by the AIP Publishing LLC.

CO_2 and Er:YAG laser interaction with grass tissues

Jaehun Kim and Hyungson Ki[a)]
School of Mechanical and Advanced Materials Engineering, Ulsan National Institute of Science and Technology (UNIST), Ulsan, South Korea

(Received 6 November 2012; accepted 7 January 2013; published online 23 January 2013)

Plant leaves are multi-component optical materials consisting of water, pigments, and dry matter, among which water is the predominant constituent. In this article, we investigate laser interaction with grass using CO_2 and Er:YAG lasers theoretically and experimentally, especially targeting water in grass tissues. We have first studied the optical properties of light absorbing constituents of grass theoretically, and then have identified interaction regimes and constructed interaction maps through a systematic experiment. Using the interaction maps, we have studied how interaction regimes change as process parameters are varied. This study reveals some interesting findings concerning carbonization and ablation mechanisms, the effect of laser beam diameter, and the ablation efficiency and quality of CO_2 and Er:YAG lasers. © *2013 American Institute of Physics*. [http://dx.doi.org/10.1063/1.4788821]

I. INTRODUCTION

Laser material interaction exhibits as diverse and complex physical phenomena as the kinds of materials and lasers involved.[1–6] In recent years, laser interaction with biological tissues has become an important research topic. Biological tissues are multi-component composite systems and are much more difficult to study in comparison to common engineering materials: they are hard to manipulate, and accurate optical properties are not available. In fact, this area has been limited to human tissues because of numerous medical applications.[7]

In a recent article by the authors,[8] for the first time, laser interaction with green plant leaves was studied systematically using 355, 532, and 1064 nm picosecond lasers and Kentucky bluegrass. As well known, grass is not only an important landscaping and agricultural material but is also an important biomass material.[9] Just like laser interaction with human and animal tissues has become an important subject in medical areas, we believe that laser interaction with plant leaves could be as important in landscaping, agricultural, and biomass areas. For instance, the effective and damage-free cutting of biomaterials are always an important issue, and an in-depth understanding of laser grass-tissue interaction can be used to develop a laser-based technology for cutting grass (or plant leaves in general).

This article is Part II of the authors' investigation into laser interaction with grass tissues. In Part I of this study,[8] we found that for $\lambda = 355$ and 532 nm, laser interacts predominantly with chlorophylls and for $\lambda = 1064$ nm dry matter is the primary light absorbing constituent of grass. Therefore, at these wavelengths, light is absorbed primarily by grass tissues. In the present article, we investigate how a laser interacts with grass tissues in the wavelength region where light absorption occurs predominantly by water, because water is the largest constituent of plant leaves. Apparently, significantly different interaction phenomena are expected when interaction mechanisms are changed. For these purposes, we have chosen Er:YAG ($\lambda = 2.94\ \mu$m) and CO_2 lasers ($\lambda = 10.6\ \mu$m) for experiments because they are known to have very high water absorptivity. To be consistent with the authors' previous research, Kentucky bluegrass (*Poa pratensis*) has been used. Note that grass is a monocotyledon and has a relatively simple leaf mesophyll structure. In this study, we have first studied optical properties of grass constituents theoretically and conducted experiments systematically to identify interaction regimes and construct interaction maps. The constructed interaction maps show how a particular process regime changes as the process parameters are varied. Scanning electron microscopy (SEM) and optical microscopy are employed for studying morphological and structural changes in grass tissues after laser irradiation. This study reveals interesting findings regarding carbonization and ablation mechanisms, the effect of laser beam diameter, and the ablation efficiency and quality of CO_2 and Er:YAG lasers.

II. THEORETICAL INVESTIGATION OF GRASS OPTICAL PROPERTIES

Grass is a multi-component optical system, and it is composed of many components with different optical properties. In our previous study,[8] we considered grass as a complex optical system consisting of two types of pigments (i.e., chlorophylls and carotenoids), water, and dry matter.[10] Because water constitutes an average of 66.4% of plant leaves[11] and the primary objective of this work is to study laser grass interaction targeting water contained in grass, we need to first understand how the absorption of light by water changes as wavelength varies. Figure 1 shows the absorption coefficient of water from 300 nm to around 11.5 μm, which is reconstructed by using the data given in Hale and Querry.[12] As shown, past the minimum at around 475 nm, the absorption coefficient increases overall as the wavelength increases and has a maximum at around 2.95 μm. Thus, the Er:YAG laser

[a)]Author to whom correspondence should be addressed. Electronic mail: hski@unist.ac.kr.

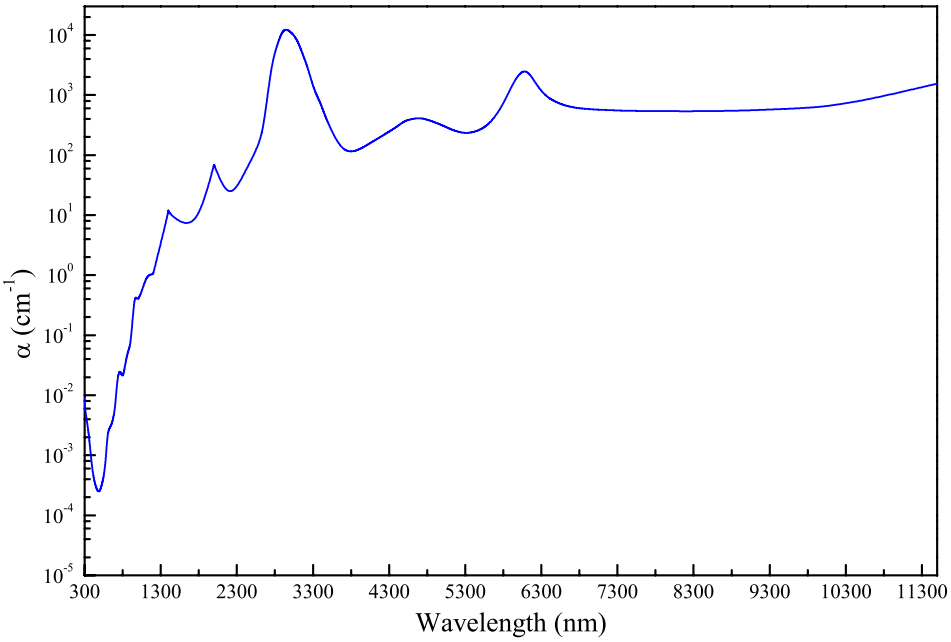

FIG. 1. The absorption coefficient of water versus wavelength (constructed using the data in Ref. 12).

at $\lambda = 2.94\,\mu$m has the highest water absorption coefficient ($\sim$12 000/cm^{-1}) among all commercially available lasers, and the CO_2 laser at $\lambda = 10.6\,\mu$m has a coefficient that is 13.95 times lower ($\sim$860/cm^{-1}) than Er:YAG laser but is still at least 3 orders of magnitude higher than 355, 532, and 1064 nm lasers.[7]

To compare the light absorption performance of various grass constituents, we calculated the $a \times C$ values for chlorophylls, carotenoids, dry matter, and water in this study. Here, a is the specific absorption coefficient (cm^2/mg) and C is the concentration of the constituent in grass per unit area of grass blade (mg/cm^2). (Note that, unlike water, the absorption coefficients of pigments and dry matter are normally defined as functions of their concentrations in plant biochemistry, so for comparison the absorption coefficient of water given in Figure 1 is converted to the specific absorption coefficient (a) using the density of water.) Therefore, $a \times C$ represents the actual absorption by each grass constituent taking into account grass composition and thickness.[8] The optical properties of plant leaves considering leaf mesophyll structures have been studied mainly for remote sensing applications.[11,13,14] In this study, specific absorption coefficients of chlorophylls (a_{chl}) and carotenoids (a_{car}) were obtained from Ref. 10, and the specific absorption coefficient of dry matter (a_{dm}) was obtained from Olioso *et al.*'s work,[15] where the authors calculated the specific absorption coefficient of dry matter in the thermal infrared region by inverting the leaf optical property model, PROSPECT,[13,14] against leaf spectrum data. The concentrations of water, chlorophylls, carotenoids, and dry matter for Kentucky bluegrass are adopted from Ref. 8 and summarized in Table I.

TABLE I. Concentrations of water, chlorophylls, carotenoids, and dry matter in a typical Kentucky bluegrass blade (expressed as mass contained in unit surface area of grass blade).

C_w (mg/cm^2)	C_{chl} (mg/cm^2)	C_{car} (mg/cm^2)	C_{dm} (mg/cm^2)
3.82	0.0393	0.00458	1.94

Figure 2 presents the $a \times C$ curves for chlorophylls, carotenoids, dry matter, and water from $\lambda = 300$ nm to 14 μm. In this figure, the $a \times C$ curve for dry matter predicted by using Olioso *et al.*'s work is shown in red. For comparison, the $a \times C$ curve for dry matter that is estimated using the data available in Maier's work[10] is shown in pink solid line. Note that this data are only available up to $\lambda = 2.5\,\mu$m and both agree reasonably well from 500 nm to 2.5 μm. One thing to note in Figure 2 is that in the wavelength range from $\sim$2.5 μm to 14 μm water is the dominant light absorbing element except around 3.6 μm, where dry matter and water absorb light almost equally. Also, in this range, the strength of light absorption by water is comparable to that of chlorophylls (and total pigments) in the near UV and visible spectrum.

In Table II, the $a \times C$ values for water, chlorophylls, carotenoids, and dry matter at $\lambda = 2.94\,\mu$m and 10.6 μm are listed, along with those values for 355, 532, and 1064 nm for comparison purposes. Here, the 355, 532, and 1064 nm values are adopted from the authors' previous work.[8] Comparing the $a \times C$ values for water and dry matter at 2.94 μm and 10.6 μm, water has 309 and 8.3 times larger $a \times C$ values than dry matter, respectively, so for these two wavelengths we can assume that water is the dominant light absorbing component. However, although the absorption by dry matter could be completely neglected for the Er:YAG laser, we believe that the amount of CO_2 laser absorption by dry matter could become significant in some situations.

In Table II, the total $a \times C$ values (i.e., $\sum_i a_i \times C_i$) are also summarized. As shown, the total $a \times C$ value for 10.6 μm is 3.70, which is close to that of 355 nm wavelength light, 2.88. Er:YAG laser at 2.94 μm has the largest value of 49.0, which is 17 times larger than that of 355 nm light. Also in the table, we estimated the effective optical penetration depth (δ) using the average grass blade thickness (ℓ_{grass}) of 110 μm as follows:[8]

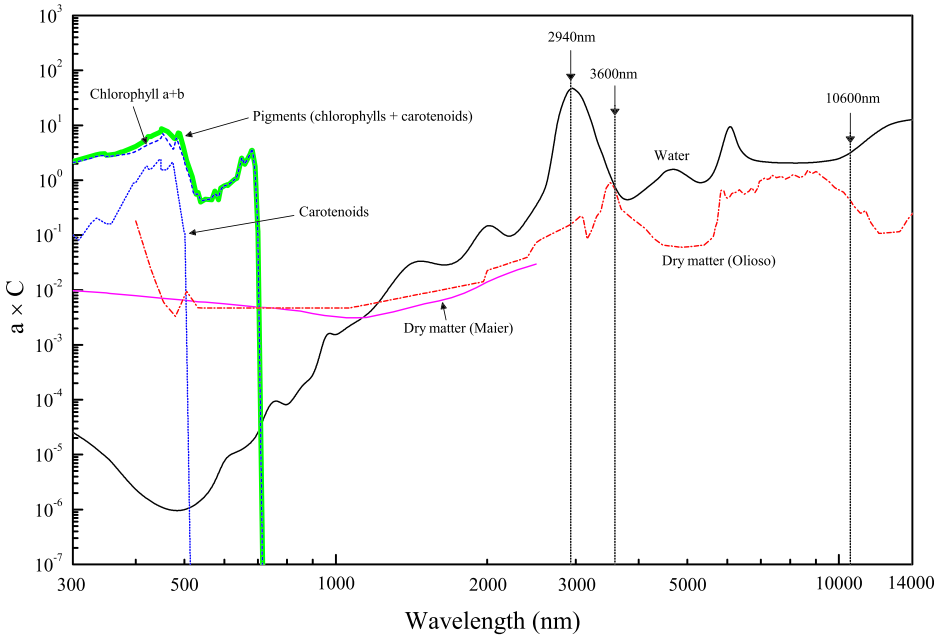

FIG. 2. Spectral absorption characteristics ($a \times C$) of major constituents of Kentucky bluegrass accounting for the thickness of grass blades.

$$\delta = \frac{1}{\alpha_{grass}} \approx \frac{\ell_{grass}}{\sum_i a_i C_i}. \quad (1)$$

This is the penetration depth for grass considering the grass composition, and for Er:YAG and CO_2 lasers, δ is 2 μm and 30 μm, respectively. Considering the fact that the corresponding δ values for pure water are 0.83 μm and 11.6 μm, respectively, and knowing that the average water content in plant leaves is reportedly 66.4%,[11] this estimation seems to be reasonable. Also, note that if the total $a \times C$ value is equal to unity, δ is the same as the grass thickness, and we can say that the most of light that enters into grass is absorbed as it reaches the bottom grass surface. Hence, we will define the *critical penetration depth* (δ_{crit}) as the thickness of the grass blade, which occurs when $\sum_i a_i \times C_i = 1$. As shown in Table II, for $\lambda = 355$ nm, 2.94 μm, and 10.6 μm, δ is smaller than δ_{crit} and we can assume that the energy of the transmitted light is almost entirely absorbed by grass within a single pass of light. Besides, for $\lambda = 355$ nm and 10.6 μm, optical penetration depths are very close at 38 μm and 30 μm, which are roughly 1/3 of the thickness of grass. On the other hand, for $\lambda = 2.94$ μm the penetration depth is only $\sim$2 μm, which is only 2% of the grass thickness.

In this study, another important optical property is spectral absorptance of grass. Absorptance data of grass, especially in the infrared region, is difficult to find, and in this study, the reflectance of green grass obtained by using the advanced spaceborne thermal emission reflection radiometer (ASTER) was employed, which is a multi-spectral imager and covers the visible, near infrared, short wavelength infrared, and thermal infrared parts of the electromagnetic spectrums.[16,17] This reflectance data are summarized in bold in Table III. Note that for $\lambda = 355$, 532, and 1064 nm the reflectance, transmittance, and absorptance data that are calculated by the leaf model, SLOPE, for banana leaves, linden leaves, and maple leaves[10] are given in parentheses. These values were used for the authors' previous work on 355, 532, and 1064 nm laser interaction with grass tissues.[8] As shown clearly in the table, the ASTER reflectance data for these three wavelengths are reasonably close to the predictions by the SLOPE model. Also, note that the reflectance values for $\lambda = 2.94$ μm and 10.6 μm are both less than 2%. Knowing that δ is less than 1/3 of the grass blade thickness for both wavelengths, we can safely assume that transmittance is virtually zero and absorptance is larger than 98% for both wavelengths. One interesting thing is that optical properties of grass for $\lambda = 355$ nm and 10.6 μm are very similar except for how light

TABLE II. The $a \times C$ values for water, chlorophylls, carotenoids, and dry matter, and the effective optical penetration depths. (The values for $\lambda = 355$, 532, and 1064 nm are adopted from Ref. 8.)

λ	$a_w C_w$	$a_{chl} C_{chl}$	$a_{car} C_{car}$	$a_{dm} C_{dm}$	$\sum_i a_i C_i$	δ (μm)
355 nm	0.0000080	2.71	0.160	0.0087	**2.88**	38
532 nm	0.0000013	0.593	0	0.0060	**0.60**	183
1064 nm	0.0023	0	0	0.0031	**0.0054**	20 370
2.94 μm	48.8	0	0	0.158	**49.0**	2
10.6 μm	3.3	0	0	0.396	**3.70**	30

TABLE III. Green grass reflectance (from the ASTER library 2.0 (Refs. 16 and 17), shown in bold face) and estimated transmittance and absorptance values. In parentheses are calculated leaf reflectance, transmittance, and absorption data averaged for banana leaves, linden leaves, and maple leaves.[8,10]

λ	R	T	A
355 nm	(0.03 $\sim$ 0.04) **0.034**	($\sim$0)	(0.96 $\sim$ 0.97)
532 nm	(0.06 $\sim$ 0.11) **0.097**	(0.08 $\sim$ 0.15)	(0.76 $\sim$ 0.86)
1064 nm	(0.42 $\sim$ 0.50) **0.525**	(0.46 $\sim$ 0.54)	(0.04 $\sim$ 0.07)
2.94 μm	**0.013**	$\sim$0	0.987
10.6 μm	**0.019**	$\sim$0	0.981

TABLE IV. Summary of experimental conditions.

Wavelength (μm)	Power (W)	Scanning speed (mm/s)	Pulse duration (μs)	Repetition rate (Hz)	Beam size
2.94	0.01 ~ 11.7	0.02 ~ 4	350	5	1 mm
10.6	0.054 ~ 117.4	0.5 ~ 500	120	5000	180 μm, 1 mm

is absorbed by grass: for $\lambda = 355$ nm light is mostly absorbed by chlorophylls and for $\lambda = 10.6$ μm by water.

III. CLASSIFICATION OF INTERACTION REGIMES

To investigate how laser interacts with grass tissues experimentally, we used a CO_2 laser and an Er:YAG laser. The CO_2 laser has a maximum average power of 150 W and a repetition rate of 5 kHz, and the pulse duration is 120 μs (ILS 12.750DX model by Universal Laser Systems). The Er:YAG laser (Lotus series by Laseroptek) has a maximum average power of 15 W, a repetition rate of 5 Hz, and a pulse duration is 350 μs. For the CO_2 laser we experimented with two different focused beam diameters, 180 μm and 1 mm. Unfortunately, however, commercially available Er:YAG lasers are mostly for medical applications, and the laser used in this study was a medical laser for skin treatment. Because the beam was delivered through a fiber optic cable with a special handpiece, we designed and fabricated a special adapter to conduct the experiment. Due to these limitations of the Er:YAG laser, we were only able to obtain a beam diameter of 1 mm. Experimental conditions used for both lasers are summarized in Table IV. Note that, although two lasers have different operational parameters, they are both μs lasers, so that similar processing results are expected. In this study, Kentucky bluegrass with an average blade thickness of 110 ± 5 μm is selected as a target. To resolve a focusing issue related to the flexibility of grass blades, we fabricated a jig using PMMA and carefully fixed grass blades.[8]

After analyzing optical micrographs of CO_2 processed grass blades, we identified six different interaction results: no visual change, decoloration, partial cut, partial cut with carbonization, through cut, and through-cut with carbonization (See Figure 3). First of all, as discussed in Ref. 8, up to a certain threshold laser intensity, the absorbed laser energy does not cosmetically affect the grass blade and there is no noticeable visual change at the surface of the grass blade (See Figure 3(a)). As shown in Figure 3(b), however, if the laser intensity is larger than the threshold, grass turns white, indicating that pigments (chlorophylls and/or carotenoids) are damaged and light absorption pattern in the visible spectrum becomes altered. We defined this phenomenon as decoloration.[8]

As the laser energy increases further, now ablation of tissues (i.e., cutting) occurs (Figures 3(c) and 3(e)). In this case, tissue ablation is believed to occur due to the strong boiling of water followed by the localized micro-explosions.[7] If the laser energy is even higher, carbon is released and grass tissues become blackened, which is called carbonization (Figure 3(f)). One major difference between this work and the

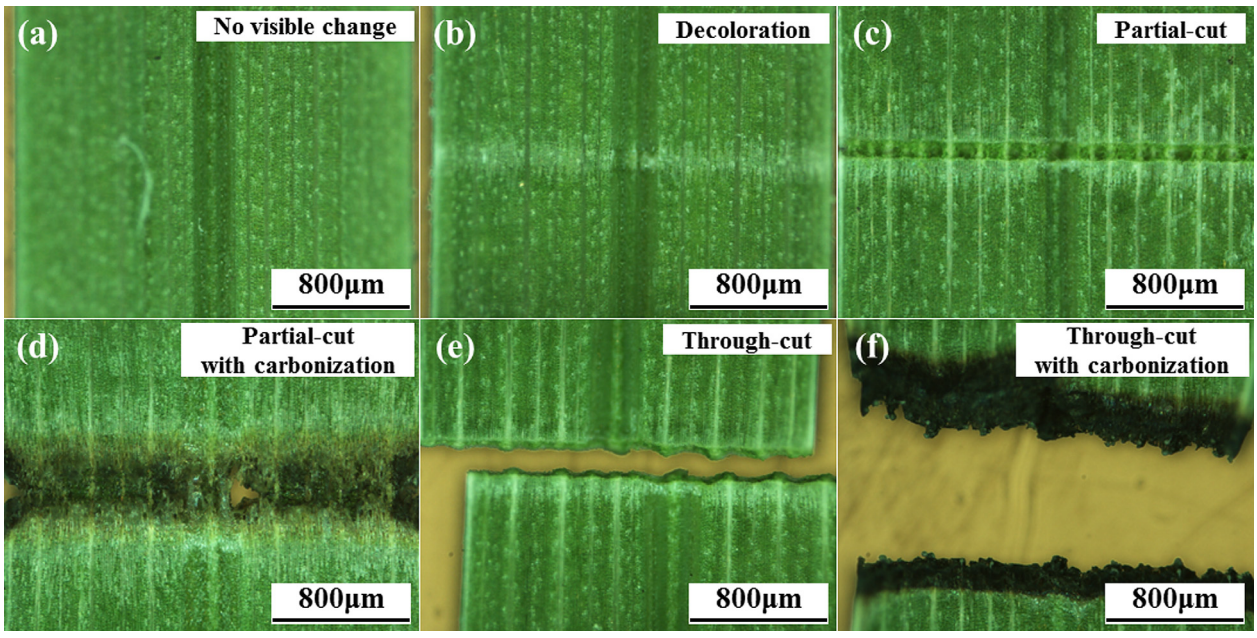

FIG. 3. Classification of interaction regimes. Although the figures were obtained from CO_2 laser interaction with grass, this classification can be applied to Er:YAG laser results. For figures (a), (b), (c), (e), (f), a beam diameter of 180 μm was used, and for figure (d) a beam diameter of 1 mm was used.

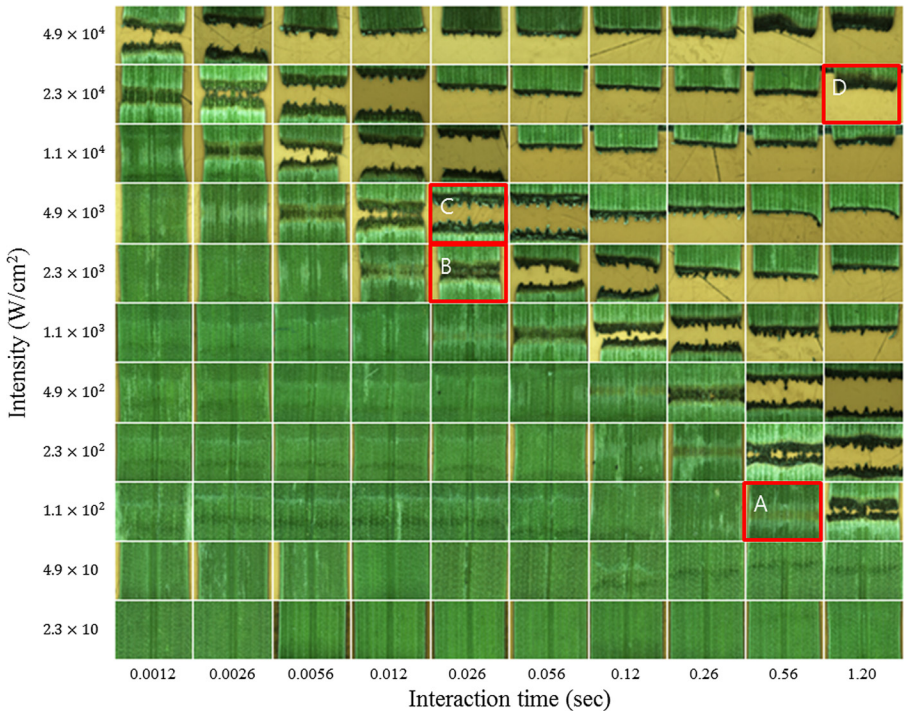

FIG. 4. Optical microscope images of grass blades after CO_2 laser irradiation with $D = 1$ mm, arranged using laser intensity and interaction time.

authors' previous work[8] is that in this work, as evidenced in Figure 3(d), carbonization was observed even when the grass was cut partially. This phenomenon was observed only when the beam diameter was 1 mm. Note that when we experimented with 355, 532, and 1064 nm picosecond lasers, we observed carbonized grass only after grass blades were completely separated. This phenomenon will be discussed in more detail in Secs. IV and V.

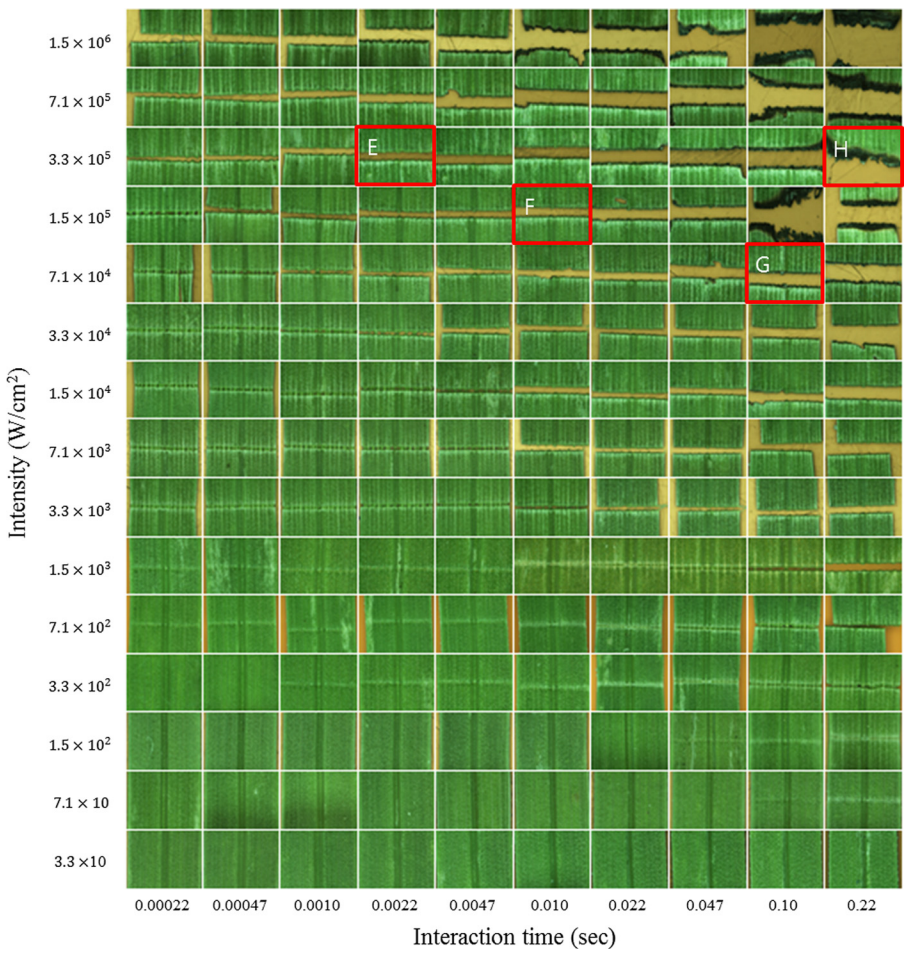

FIG. 5. Optical microscope images of grass blades after CO_2 laser irradiation with $D = 180\ \mu$m beam, arranged using laser intensity and interaction time

IV. CO_2 LASER INTERACTION MAPS AND EFFECT OF BEAM SIZE

We have first constructed interaction maps using CO_2 lasers. Apparently, peak laser intensity (I) and beam scanning speed (V_{scan}) are primary process parameters, and we attempted to cover as wide a process range as possible within the limitations of the equipment. (The ranges of laser power and scanning speed are summarized in Table IV.) In this study, in order to investigate the effect of beam diameter, we conducted the experiment with two different beam diameters (D), 180 μm and 1 mm. Because the water content in grass could vary throughout the year, experiments were conducted in two successive days in order to avoid seasonal effects ($D = 180\,\mu$m experiment on June 23, 2011, and $D = 1$ mm experiment on June 24, 2011).

Figures 4 and 5 present optical microscope images of grass blades arranged according to peak laser intensity and interaction time corresponding to $D = 1$ mm and $D = 180\,\mu$m, respectively. Here, we assumed a Gaussian energy distribution ($M^2 = 1.2 \pm 0.2$) and the peak intensity is calculated as twice the average intensity. Note that we used interaction time (t_i) instead of scanning speed in order to generalize the results, and discretized the parameter space using logarithmic scales. In this study, interaction time is defined as

$$t_i = \phi \frac{D}{V_{scan}}, \tag{2}$$

where ϕ is the duty cycle of the laser. In both figures, overall, we can see that similar interaction regimes are located in the diagonal direction. The biggest difference between the two cases is that when $D = 1$ mm, as we briefly mentioned in Sec. III, carbonization occurred even when the grass was partially cut, which was not observed in the $D = 180\,\mu$m case and the authors' previous experiments with picosecond lasers. In other words, when a large beam was used grass could be carbonized before it was fully separated, but with a small beam grass was carbonized only after the grass blade was completely cut.

In order to investigate grass morphology more closely, several interaction results at different conditions are selected from Figs. 4 and 5 in the order of increasing energy density (figures in red boxes) and are presented in Figure 6 together with the corresponding SEM images. Figures 6(a)–6(d) are optical microscope and corresponding SEM images for $D = 1$ mm. Figure 6(a) shows a carbonized grass blade (blackened area) with a larger decoloration area (whitened area). The carbonization mark is not distinguishable in the corresponding SEM image, so it seems that the degree of carbonization is

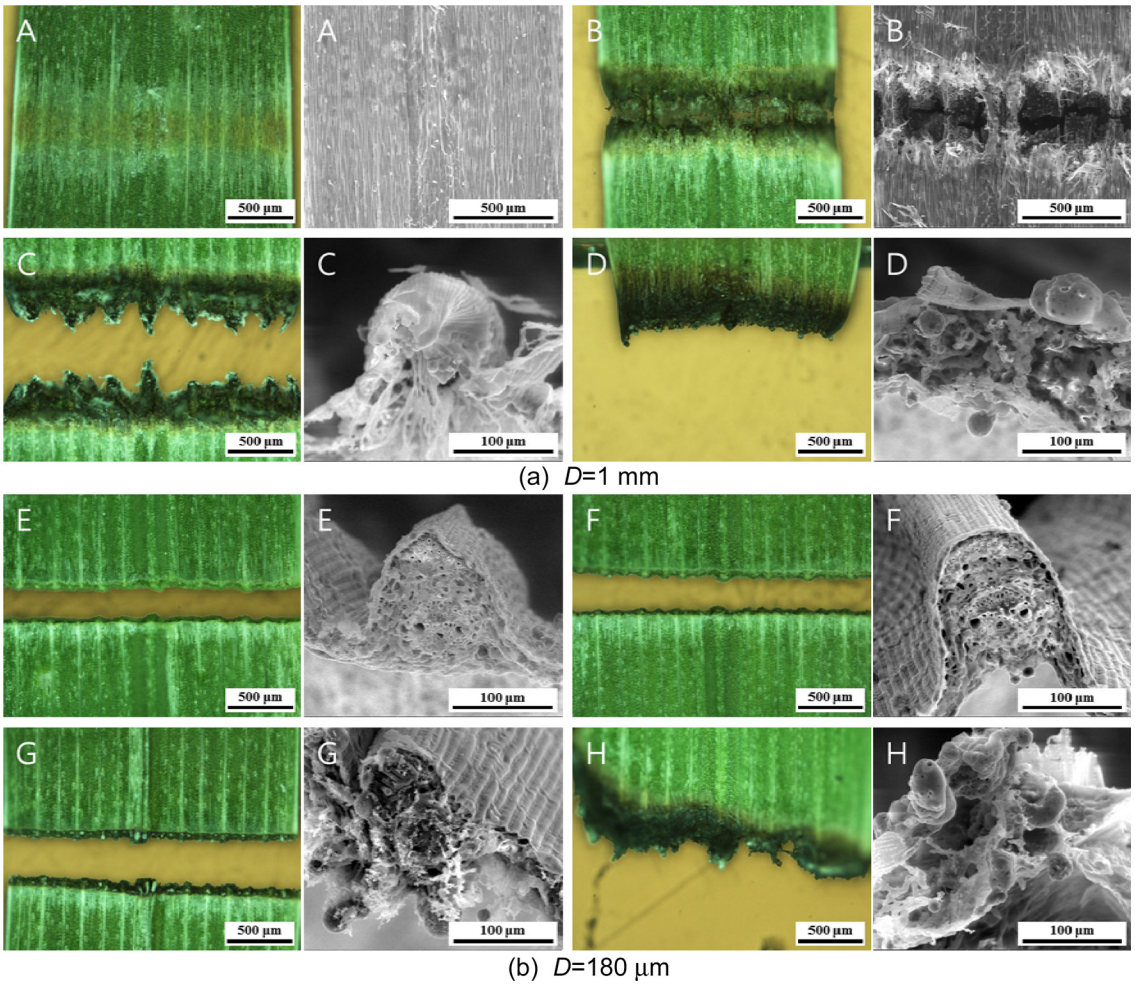

FIG. 6. Optical microscope and the corresponding SEM images for CO_2 laser processed grass blades. Figures (a) ~ (d) were obtained for $D = 180\,\mu$m, and figure (e) ~ (h) for $D = 1$ mm. The corresponding optical microscope images for these figures can be found in Figures 4 and 5.

very low and the tissue damage is minimal. In Figure 6(b) is presented a partially cut grass blade that is also carbonized. Note that in this case the partial-cut width is ~300 μm and the carbonized region width is ~600 μm. Figure 6(c) presents a grass blade that was processed with higher energy density, where the cut width is ~500 μm and the carbonized region width is ~1.2 mm. Also, the cut line is not smooth but saw-toothed. This saw-toothed cut lines can be found in most of the images in Figure 4, and we believe that it is characteristic of carbonization being dominant over ablation. One the other hand, in Figure 6(d), the cut line is relatively smooth and we believe that ablation is more dominant than carbonization. Note that as shown in SEM images, the cut regions are damaged and distorted severely due to carbonization when a partial or through cut is made with carbonization.

Figures 6(e)–6(h) are optical microscope and corresponding SEM images for 180 μm beam diameter. Figure 6(e) shows a through-cut grass image with no carbonization marks. In this case, the SEM image shows extremely clean and undamaged morphology. Figure 6(f) presents a through-cut image with very little carbonization marks. Note that in this case, the degree of carbonization is virtually zero around the cut area, so we believe that carbonization occurs by the leftover heat after the ablation process has been finished. Therefore, this kind of grass morphology will be classified as a non-carbonized grass blade in this study. The corresponding SEM image shows that the cut cross-section is still very clean with no noticeable tissue damage. As shown in Figure 6(g), however, when the energy is increased, now carbonization marks become prominent around the cut areas and the tissues become damaged as evidenced by the corresponding SEM image. Figure 6(h) shows completely carbonized and damaged grass morphology at higher laser energy.

As is obvious by now, ablation and carbonization are two primary mechanisms in the laser interaction with grass (and plant leaves), and one is more dominant than the other depending on the process parameters. Therefore, to study the interaction physics, these mechanisms must be understood first.

As we discussed earlier, when the energy transfer to grass tissues is indirect via water, ablation (or cutting) occurs due to the strong boiling of water followed by localized micro-explosions.[7] In other words, the ablation process is *mechanical* and tissues do not need to absorb energy directly to get removed. On the other hand, however, carbonization is a *thermal* process and the tissues themselves must be heated up by receiving energy from water to become carbonized.

Carbonization of grass tissues is a very complex phenomenon, and to the best of the authors' knowledge, laser induced carbonization has yet to be studied. In this study, however, because cellulose is the primary material that constitutes plant leaves, we assumed the carbonization of cellulose by pyrolysis as the major mechanism of grass tissue carbonization. Tang and Bacon in their work[18] found that during the pyrolysis of cellulose the major pyrolytic degradation begins at 240 °C and is completed at around 320 °C. Therefore, in this study, we will assume that carbonization of grass occurs in that temperature range.

On the other hand, vaporization processes during laser ablation are relatively well studied. In a typical laser ablation process, two types of vaporization processes, evaporation and homogenous boiling (or explosive boiling), could occur depending on the process parameters. In the case of water, because the normal boiling point at room temperature and the critical point temperature (T_{cp}) are only 100 °C and 374.14 °C (647.29 K),[19] respectively, both vaporization modes could easily take place at relatively low laser fluences. It is well known that the evaporation pressure increases almost exponentially towards the critical point, and according to Ref. 20, the maximum attainable pressure by surface evaporation is estimated to be $p \approx 0.333 p_{cp} \approx 74$ bar at $T \approx 0.924 T_c \approx 325$ °C, where the critical point pressure (p_{cp}) of water is 220.9 bar.[19] Meanwhile, homogeneous boiling is initiated at around $T \approx 0.9 T_{cp} \approx 309$ °C, and the maximum achievable vaporization pressure could be close to $p_{cp.}$.[20] Considering that grass tissues are tender and the laser-induced pressure force acts impulsively, we may think that both vaporization modes contribute to the cutting of grass blades over a wide temperature range. However, since carbonization has a lower threshold energy density than the ablation of grass tissues as evidenced in Figure 6(a), we believe that the actual ablation occurs at a higher temperature than ~320 °C, meaning that the ablation is primarily by homogeneous boiling.

Observing Figure 6(e), where ablation occurs without carbonization, however, it looks like ablation has lower threshold energy than carbonization, i.e., ablation occurs earlier than carbonization. Note that in this case the beam diameter is only 18% of the beam diameter used for Figure 6(a). We believe that this dominancy of ablation at a much smaller beam diameter can be explained by increased heat loss in the lateral direction. As illustrated in Figure 7, given the same laser intensity and pulse duration, we can assume that the maximum temperatures (T_0) for both cases are approximately equal and occur at the center of the laser beam. By the same token, the temperatures at the beam radius locations (T_R) are roughly the same because the intensities will be equal and the heating is very rapid. In other words, the heat flow (loss) for $D = 180$ μm is ~5.6 times (1/0.18) larger because $\dot{q}'' = -k\frac{dT}{dr} \approx k\frac{T_0 - T_R}{R}$, where R is the beam radius and k is the thermal conductivity. This greatly increased heat loss is believed to have an adverse effect on the carbonization process because it takes longer to heat up the actual grass tissues than water. Note that the heating of grass tissues occurs indirectly by the heat transfer from water after water is heated up by laser. Therefore, if the laser energy is high enough to initiate homogeneous boiling, the energy absorbed by water will be used for vaporizing water (i.e., ablating grass tissues), and carbonization occurs later with the heat transferred from water (although carbonization has the lower threshold temperature than ablation). If the energy absorbed by water is lost by conduction faster due to decreased beam diameter, it will take much larger laser energy to carbonize grass tissues. Note that a more rigorous analysis is needed to have a complete understanding of the ablation and carbonization processes, but we will leave it as a future research topic.

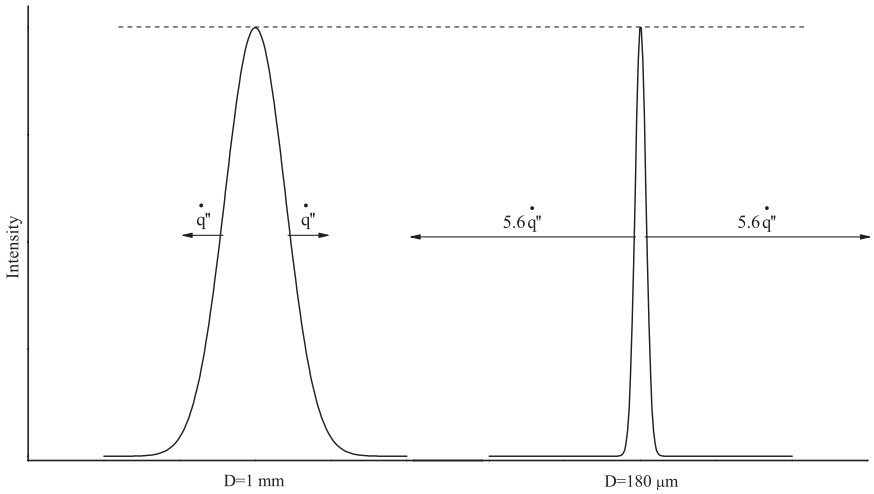

FIG. 7. Comparison of the amounts of heat loss for different beam diameters. The arrows graphically indicate the directions and magnitudes of heat loss for each beam size.

In order to study the experimental results more systematically, interaction maps were constructed from Figures 4 and 5 using the classification defined in Sec. III. In this way, we can understand how interaction regimes change as process parameters are varied. Figure 8 shows CO_2 laser interaction maps. The first and second rows show the interaction maps for $D = 180\,\mu$m and $D = 1$ mm, respectively, both of which are combined as a single plot in the third row. Note that for each case we generated two interaction maps by using interaction time (left figures) and laser energy per unit scan length (right figures) as the x-axes. In this study, laser energy per unit scan length (E') is defined as

$$E' = \frac{D_0}{D}\frac{P_{ave}}{V_{scan}}, \tag{3}$$

where D_0 is the reference beam diameter. ($D_0 = 1$ mm is chosen in this study.) In other words, we revised the previous definition of E' (Ref. 8) by multiplying a correction factor D_0/D in order to account for the beam diameter effect (with respect to 1 mm). Apparently, if a smaller beam diameter is used, given the same laser intensity and scanning speed, the processed region will become narrower and this will lead to a smaller energy to cover the same scan length. Therefore, the use of the correction factor is believed to eliminate unnecessary beam size effect in interpreting interaction maps.

In Figure 8, different interaction regimes are shown with different colors, and a red boundary line is used when carbonization has simultaneously occurred. Note that if the slope is $-45°$ on the $I - t_i$ diagram, it will appear vertical on the $I - E'$ diagram, and a horizontal line on the $I - t_i$ diagram will remain horizontal on the $I - E'$ diagram. As shown in Figures 8(a) and 8(c), as expected, interaction regimes are shaped in a way that intensity is inversely proportional to interaction time. Overall, the slopes of the interaction regimes seem to decrease from roughly $-45°$ as the interaction regime change from carbonization to no visual change. This tendency is more clearly demonstrated on the $I - E'$ diagrams (Figures 8(b) and 8(d)), where carbonization and through-cut regions are almost vertical and no-visual-change regions are close to horizontal. Therefore, we can say that the decoloration process is more sensitive to laser intensity, and the carbonization process depends more on energy density, which is in line with the authors' previous experiments on picosecond laser interaction with grass tissues.[8]

In Figures 8(e) and 8(f), the results for two different diameters are combined together. Although experimental parameters for the two cases are different due to the changed beam size, the same interaction regimes from two different maps are connected almost seamlessly except for the carbonization regimes. For $D = 1$ mm, carbonization and ablation (i.e., cutting) occur almost simultaneously, but for $D = 180\,\mu$m, carbonization occurs at a much higher energy density than ablation. This phenomenon has been already explained from a viewpoint of increased heat loss and deferred carbonization due to decreased beam diameter (See Figure 7). Comparing the two cases, there is about a 2 orders-of-magnitude difference in the carbonization threshold energy. Note that because of this beam size effect, smaller beams are much more desirable with minimized damage when processing plant leaves.

V. ER:YAG LASER INTERACTION MAPS

In this study, we have also constructed interaction maps for the Er:YAG laser. As mentioned earlier, because of the limitations of the available Er:YAG laser, only a beam diameter of 1 mm was used and grass morphology was studied by a portable optical microscope only. Note that because grass withers so quickly after it is cut, if the imaging equipment such as SEM is not located in a close enough distance from the location of the laser, it is of no use. To compare the experimental results with the CO_2 laser results, grass must be at similar conditions. To minimize seasonal effects (although it is almost unavoidable), the Er:YAG experiment was conducted on May 17, 2012, a similar time in year to the CO_2 laser experiment date (June 24, 2011).

Figure 9 presents optical microscope images of grass blades arranged according to peak laser intensity and interaction time. As shown in the figure, similar to the CO_2 laser result, the images for similar cut quality are located diagonally, and the interaction regimes changes from no visible change to decoloration to partial cut to through cut as the overall energy level increases. However, there are two

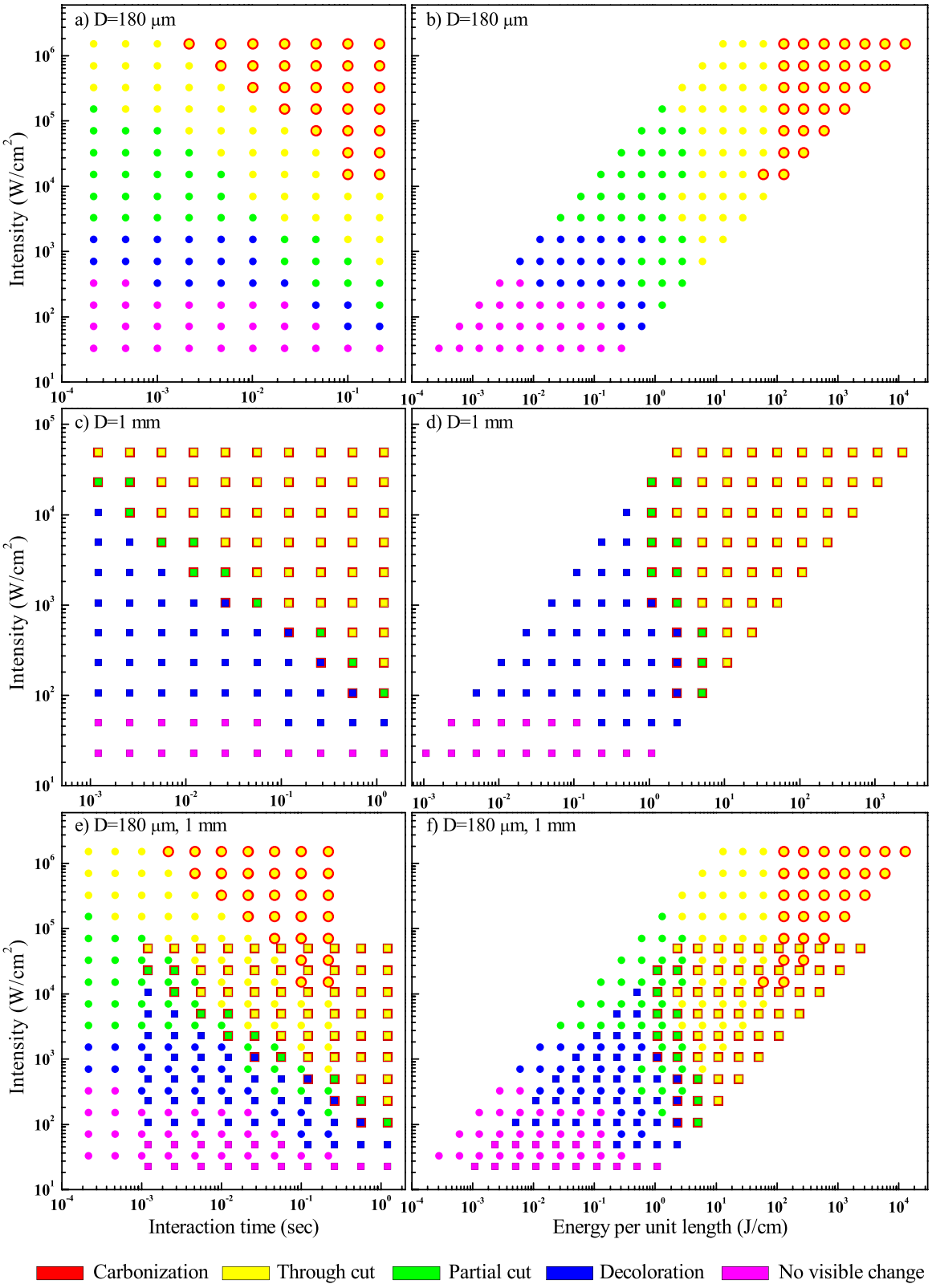

FIG. 8. CO_2 laser interaction maps for $D = 180\ \mu$m (top row) and $D = 1$ mm (middle row). In the bottom row, two results are combined as single plots.

notable differences comparing with the 1 mm CO_2 laser result. First, the overall carbonization level is much lower for the Er:YAG laser (See Figures 9 and 4). This can be explained in terms of much lower light absorptivity of dry matter at $\lambda = 2.94\ \mu$m. As discussed in Sec. II, in the case of Er:YAG laser, the $a \times C$ value for dry matter is 309 times smaller than that of water while it is only 8.3 times for the CO_2 laser. In other words, the amount of light absorption by dry matter for the Er:YAG laser is virtually negligible, which we believe may adversely affect the carbonization process.

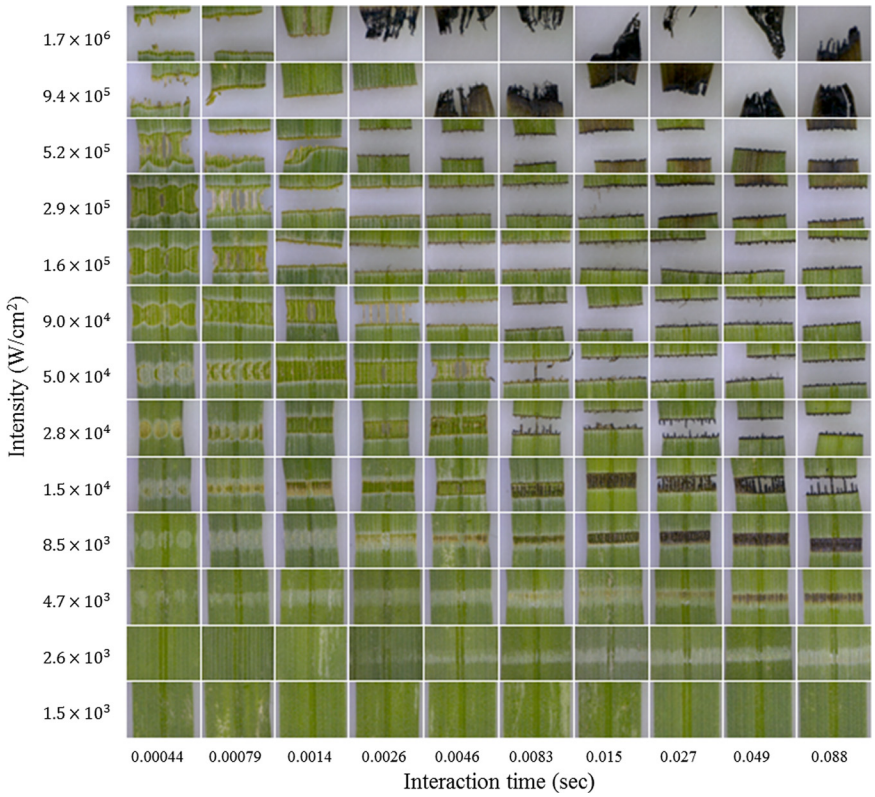

FIG. 9. Optical microscope images of grass blades after Er:YAG laser irradiation with $D = 1$ mm beam, arranged using laser intensity and interaction time.

After all, grass tissues (i.e., dry matter) must be heated up to be carbonized. For the CO_2 laser interaction, dry matter could absorb a non-negligible amount of energy and this energy will mostly contribute to carbonization. Furthermore, this is a direct heating and not via water, so it increases the tissue temperature much faster.

The second major difference is that, in the case of Er:YAG laser, even along the diagonal line (i.e., at the same energy density) the degree of carbonization varies. As clearly shown in Figure 9, with respect to an interaction time of around 0.006 s, carbonization is much more conspicuous on the right side, and on the left we can notice very little carbonization. Note that, for the CO_2 laser, as shown in Figures 4 and 5, the degree of carbonization is nearly uniform diagonally. We believe that this remarkable difference is caused by the very low duty cycle of the Er:YAG laser: the duty cycle of Er:YAG laser is only 0.00175 (350 μs pulse width, 5 Hz repetition rate) while the CO_2 laser has a duty cycle of 0.6 (120 μs pulse width, 5000 Hz repetition rate). If the duty cycle is 0.6, the effect of a pulse on the next pulse is significant, so that the laser might be considered semi-continuous. However, if the duty cycle is 0.00175, the effect of a pulse on the next one is virtually zero. In order to validate this explanation, we simulated laser interaction with water using a simple one-dimensional heat conduction model[21] employing the same laser parameters used in the experiments. The density, thermal conductivity, and thermal diffusivity of water are assumed to be 1000 kg/m^3, 0.6 W/m·K, and 0.143×10^{-6} m^2/s, respectively, and a laser intensity of 4×10^3 W/cm^2 is used. Figure 10 presents the simulation results and validates the authors' predictions on the effect of duty cycle for both lasers. If the pulse effect cannot be accumulated due to the

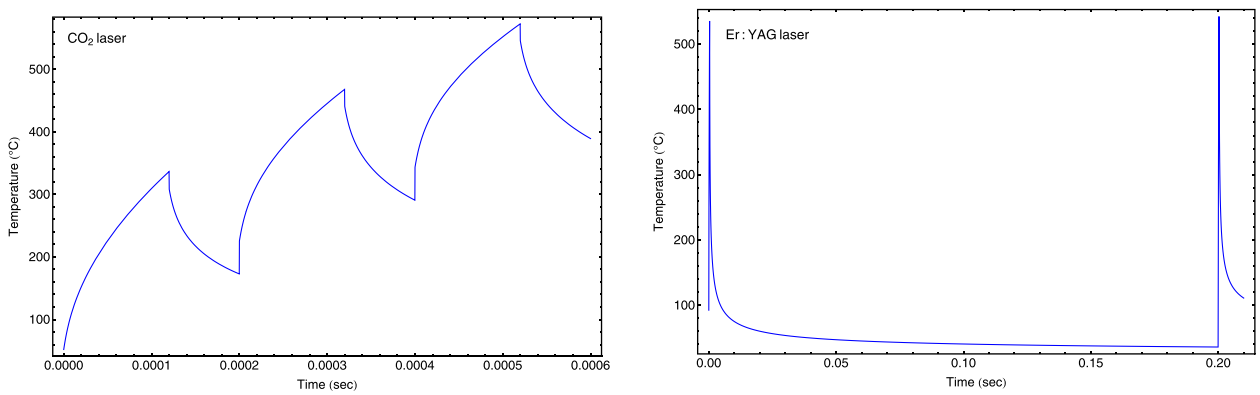

FIG. 10. Heating patterns of water by CO_2 laser (left) and Er:YAG laser (right) simulated using a one-dimensional heat conduction model. $I = 4 \times 10^3$ W/cm^2 was assumed.

very small duty cycle, now the temperature rise is determined solely by the laser intensity (at the fixed pulse width). Therefore, in the case of Er:YAG laser, when interaction time is small (i.e., high laser intensity) temperature rises higher and ablation becomes more dominant, and when interaction time is large (i.e., low laser intensity) temperature is lower and carbonization becomes dominant due to the elongated heating time. Note that for the carbonization process a longer pulse width is more favorable.

In order to study the experimental results more closely, interaction maps were constructed using the classification of interaction regimes defined in Sec. III. In Figure 11, Er:YAG laser interaction maps are shown in the top row, and in the bottom row, we present combined plots of Er:YAG laser and 1 mm CO_2 laser results. Note that laser intensity and laser energy per unit scan length are used as the x-axes in the left and right figures, respectively.

The overall distribution of interaction regimes is similar to that of CO_2 laser: carbonization and through-cut thresholds are determined by energy density per unit scan length and decoloration is more sensitive to laser intensity (See Figures 11(a) and 11(b)). However, as shown in Figure 11(b), although the carbonization region exists across the partial-cut and through-cut regions, it is located only at the lower intensity part. This was explained in connection with the very small duty cycle of the Er:YAG laser.

Comparing interaction maps for CO_2 and Er:YAG lasers (Figures 11(c) and 11(d)), we can notice that, although different lasers were used, the two interaction maps are matched reasonably well. However, there are three major mismatches: the Er:YAG laser seems to have higher threshold values for carbonization, decoloration, and through-cut processes. In other words, the Er:YAG laser are less efficient than the CO_2 laser in spite of its 13.95 times higher water absorption coefficient. As discussed earlier in Sec. II, however, the absorptance of light in grass at 2.94 μm and 10.6 μm are very close (>0.98, See Table III), so that there is virtually no difference in terms of the amount of absorbed energy. In this case, one factor that affects carbonization and decoloration more is believed to be the light absorption by dry matter because both processes are processes of modifying grass tissues. In the case of the Er:YAG laser, the heating of grass tissues (i.e., dry matter) is almost entirely by the heat transfer from water, higher

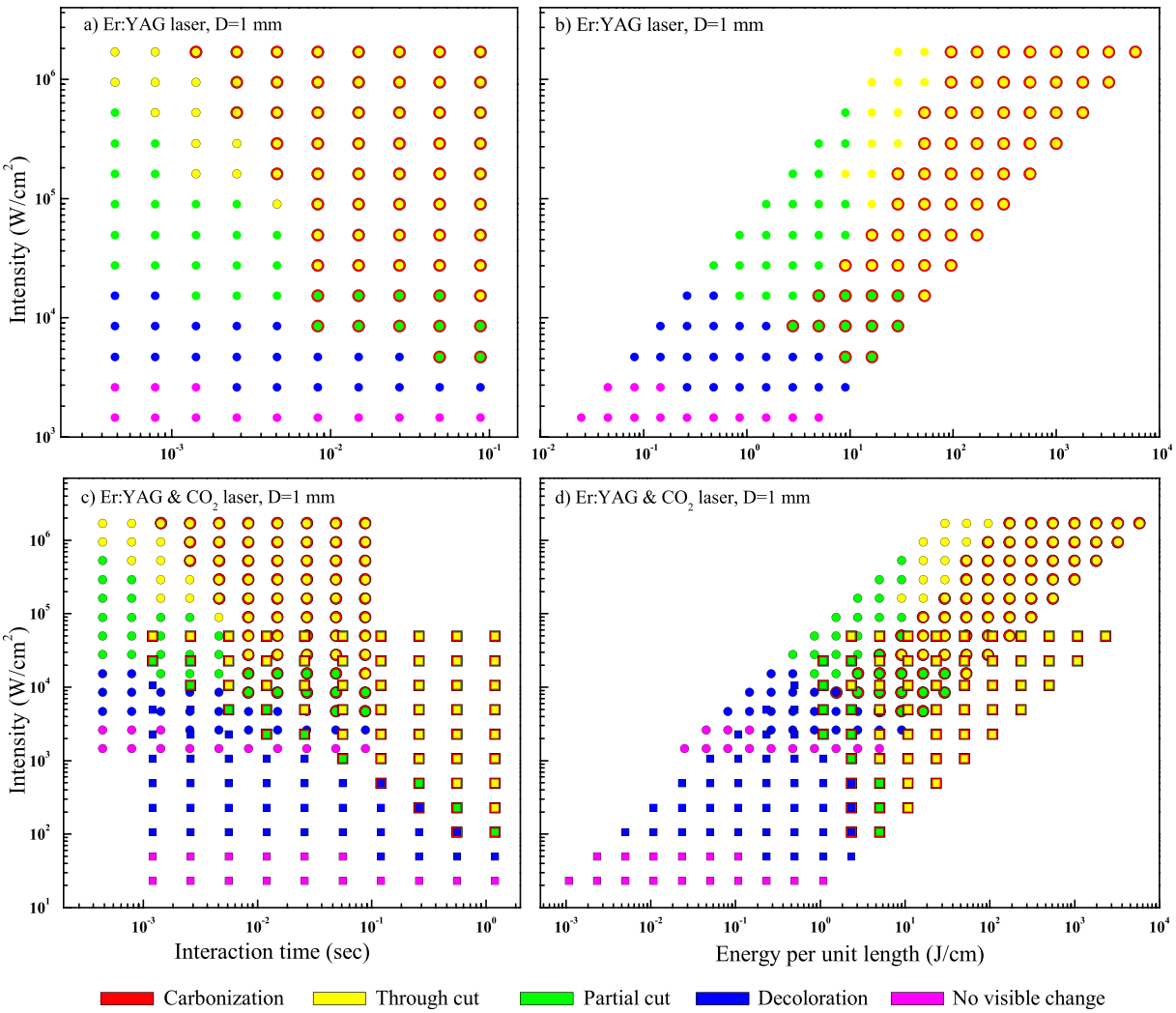

FIG. 11. Top figures: Er:YAG laser interaction maps. Bottom figures: CO_2 and Er:YAG laser interaction maps combined together (circles: Er:YAG laser, squares: CO_2 laser). $D = 1$ mm for all interaction maps.

laser energy might be required compared to the CO_2 laser processing.

The cutting of grass, however, is a mechanical process due to vaporization of water, so the higher through-cut threshold energy for the Er:YAG laser is rather surprising. We believe that this is ascribed to the much smaller optical penetration depth of the Er:YAG laser. As estimated in Table II, the optical penetration depths of Er:YAG and CO_2 lasers are 30 μm and 2 μm, respectively. Note that, regardless of the pulse energy, the amount of ablated tissues will be strongly affected by the depth of the region where energy is absorbed, which means that the Er:YAG laser is less efficient than the CO_2 laser even for the ablation process. In other words, the Er:YAG laser may require more laser pulses to separate a grass blade. In spite of the difference in through-cut threshold energies, however, we can notice from Figure 11(d) that the partial-cut threshold energy values for the two lasers are similar. This is reasonable because the partial-cut threshold is the laser energy density at which ablation is first observed and, hence, is not dependent on the optical penetration depth.

VI. CONCLUSION

In this study, CO_2 and Er:YAG laser interaction with grass tissues was studied theoretically and experimentally. In both cases, the absorption of light is dominated by water and the amount of light absorption is >98%. In this study, we found that to reduce tissue damage due to carbonization, a laser beam with a smaller diameter needs to be used. Furthermore, the Er:YAG laser is better the CO_2 laser in terms of minimized tissue damage but has higher threshold laser energy and intensity due to the very small energy absorption by dry matter and the thin optical penetration depth.

ACKNOWLEDGMENTS

This research was supported by the Basic Science Research Program through the National Research Foundation (NRF) of Korea funded by the Ministry of Education, Science and Technology (Grant No. 2010-0005744). We also would like to appreciate Laseroptek corporation located in Sungnam, Korea for their generous permission to use their Lotus Er:YAG laser system.

[1]S. Heiroth, J. Koch, T. Lippert, A. Wokaun, D. Gunther, F. Garrelie, and M. Guillermin, "Laser ablation characteristics of yttria-doped zirconia in the nanosecond and femtosecond regimes," J. Appl. Phys. **107**, 014908 (2010).
[2]R. Ortiz, I. Quintana, J. Etxarri, A. Lejardi, and J. R. Sarasua, "Picosecond laser ablation of poly-L-lactide: Effect of crystallinity on the material response," J. Appl. Phys. **110**, 094902 (2011).
[3]J. Kolar, M. Strlic, D. Muller-Hess, A. Gruber, K. Troschke, S. Pentzien, and W. Kautek, "Near-UV and visible pulsed laser interaction with paper," J. Cultural Heritage **1**, S221–S224 (2000).
[4]J. Kolar, M. Strlic, S. Pentzien, and W. Kautek, "Near-UV, visible and IR pulsed laser light interaction with cellulose," Appl. Phys. A **71**, 87–90 (2000).
[5]D. J. Lim, H. Ki, and J. Mazumder, "Mass removal modes in the laser ablation of silicon by a Q-switched diode-pumped solid-state laser (DPSSL)," J. Phys. D **39**, 2624–2635 (2006).
[6]H. Li and H. Ki, "Effect of ionization on femtosecond laser pulse interaction with silicon," J. Appl. Phys. **100**, 104907 (2006).
[7]M. H. Niemz, *Laser-Tissue Interactions: Fundamentals and Applications*, 3rd, enlarged ed. (Springer-Verlag, Berlin, Germany, 2004).
[8]J. Kim and H. Ki, "355, 532, and 1064 nm picosecond laser interaction with grass tissues," J. Appl. Phys. **112**, 114908 (2012).
[9]J. L. Xu, Z. Y. Wang, and J. J. Cheng, "Bermuda grass as feedstock for biofuel production: A review," Bioresource Technol. **102**, 7613–7620 (2011).
[10]S. W. Maiser, "Modeling the radiative transfer in leaves in the 300 nm to 2.5 um wavelength region taking into consideration chlorophyll fluorescence—the leaf model SLOPE," Ph.D. dissertation, Technische University Munchen, Germany, 2000.
[11]S. Jacquemoud, S. L. Ustin, J. Verdebout, G. Schmuck, G. Andreoli, and B. Hosgood, "Estimating leaf biochemistry using the PROSPECT leaf optical properties model," Remote Sens. Environ. **56**, 194–202 (1996).
[12]G. M. Hale and M. R. Querry, "Optical-constants of water in 200-nm to 200-um wavelength region," Appl. Opt. **12**, 555–563 (1973).
[13]S. Jacquemoud and F. Baret, "PROSPECT: A model of leaf optical-properties spectra," Remote Sens. Environ. **34**, 75–91 (1990).
[14]J. B. Feret, C. Francois, G. P. Asner, A. A. Gitelson, R. E. Martin, L. P. R. Bidel, S. L. Ustin, G. le Maire, and S. Jacquemoud, "PROSPECT-4 and 5: Advances in the leaf optical properties model separating photosynthetic pigments," Remote Sens. Environ. **112**, 3030–3043 (2008).
[15]A. Olioso, S. Jacquemoud, and F. Baret, see http://www.ipgp.fr/~tarantola/exercices/chapter_05/RadiativeModel/OldRadiativeModel/S2.02.AOlioso.ppt for adaptation of the leaf optical property model PROSPECT to tehrmal infrared.
[16]A. M. Baldridge, S. J. Hook, C. I. Grove, and G. Rivera, "The ASTER spectral library version 2.0," Remote Sensing of Environment **113**, 711–715 (2009).
[17]NASA, see http://speclib.jpl.nasa.gov for ASTER spectral library.
[18]M. M. Tang and R. Bacon, "Carbonization of cellulose fibers.1. Low temperature pyrolysis," Carbon **2**, 211–220 (1964).
[19]M. J. Moran and H. N. Shapiro, *Fundamentals of Engineering Thermodynamics*, 6th ed. (Wiley, 2008).
[20]H. Ki, "On vaporization in laser material interaction," J. Appl. Phys. **107**, 104908 (2010).
[21]H. Ki and S. So, "Process map for laser heat treatment of carbon steels," Opt. Laser Technol. **44**, 2106–2114 (2012).